

Supporting Information

Performance enhancement of single-walled carbon nanotube – microwave exfoliated graphene oxide composite electrodes using a stacked electrode configuration.

Dennis Antiohos¹, Mark S. Romano¹, Joselito M. Razal¹, Stephen Beirne¹, Phil Aitchison², Andrew I. Minett³, Gordon G. Wallace¹, Jun Chen^{1*}

¹Intelligent Polymer Research Institute ARC Centre of Excellence for Electromaterials Science, University of Wollongong, NSW, 2522, Australia

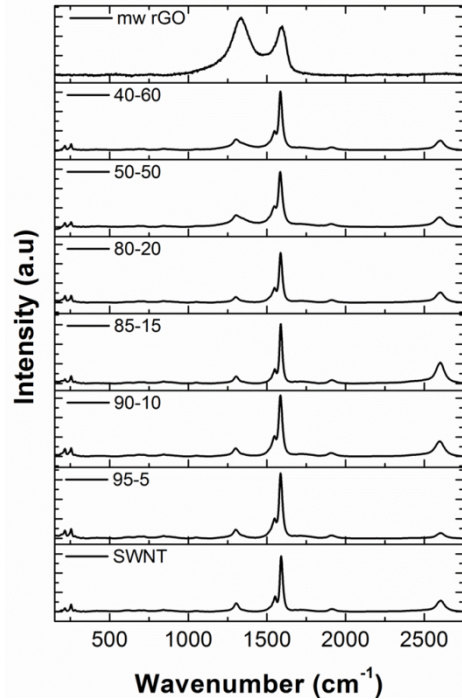
²CAP-XX Australia Pty Ltd, Lane Cove, NSW, 2066, Australia

³School of Chemical and Biomolecular Engineering, University of Sydney, NSW, 2006, Australia

E mail: junc@uow.edu.au

Table S1: Comparison of radial breathing modes and D/G band ratio for SWNT – mw rGO composite electrodes before and after 20 minutes plasma treatment.

%Composition of SWNT:mw rGO (w/w)	Before treatment	Before treatment	Plasma treated	Plasma treated	D/G Before	D/G plasma treated
	d ^{1st} peak (nm)	d ^{2st} peak (nm)	d ^{1st} peak (nm)	d ^{2st} peak (nm)		
100:0	1.149	0.969	1.153	0.974	0.116	0.150
95:5	1.147	0.970	1.151	0.974	0.109	0.138
90:10	1.149	0.973	1.152	0.973	0.106	0.133
85:15	1.151	0.972	1.152	0.974	0.111	0.118
80:20	1.147	0.970	1.149	0.973	0.096	0.114
50:50	1.149	0.970	1.152	0.974	0.186	0.212
40:60	1.147	0.971	1.154	0.974	0.182	0.229
0:100	-	-	-	-	1.168	1.240



19

20 **Figure S1: Raman spectroscopy of SWNT-mw rGO composite electrodes after 20 minutes plasma treatment. Laser line**
 21 **used was 632.81 nm.**

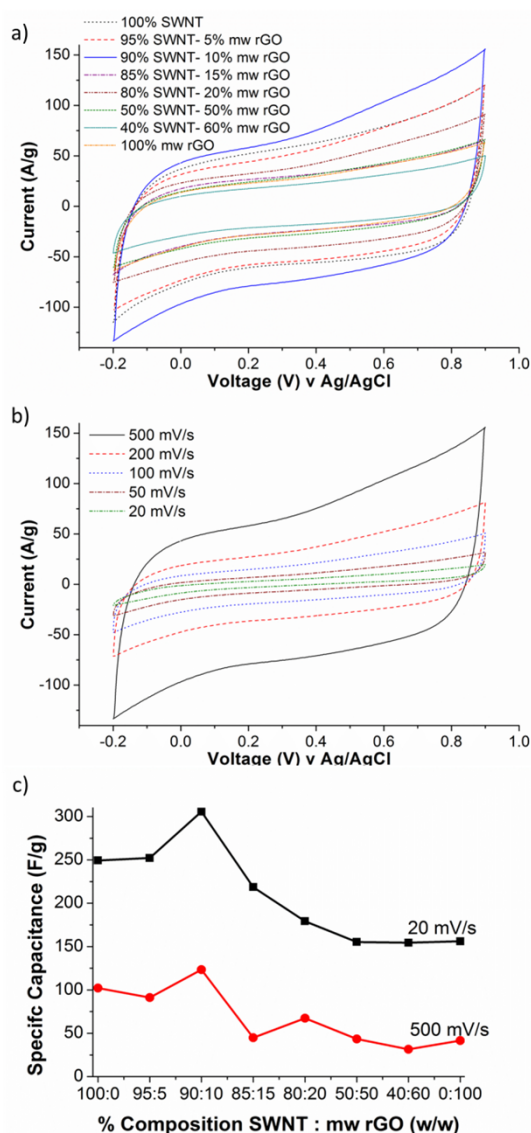
22

23 Before and after plasma treatment the D/G ratio of SWNT is 0.116 and 0.150 respectively indicates a high degree
 24 of purity for the SWNTs [1, 2]. The shoulder peak (1553 cm^{-1}) to the left of the G band (1591 cm^{-1}) is most likely from the
 25 effect of functional groups on the sp^2 breathing mode [1]. As the ratio of SWNT is decreased (and subsequently mw rGO is
 26 increased) it can be seen that the D band of the composite broadens. This broadening is thought to be two D band peaks
 27 associated with SWNT and mw rGO with the D band of the mw rGO becoming stronger as its weight ratio is increased. It
 28 can be seen from Figure S1 that there is an extremely small difference in the D/G band ratio of the Raman spectra for the
 29 samples prior to and after plasma treatment. This may suggest that the plasma treatment is sufficient enough to provide an
 30 enhanced wettability of the electrode surface, but there are no significant alterations to the materials structure [3]. It can
 31 be seen that the 100% SWNT shows small bundles of SWNTs that form the film, with calculation of the SWNT bundle size
 32 estimated in Table 1 for all composites [4]. The SWNT bundle diameters have only increased very marginally indicating a
 33 uniform and very well formed suspension between SWNT and mw rGO has still occurred.

34

35

36



37

38 **Figure S2: SWNT : mw rGO composite electrode. (a) Cyclic voltammetry at 500 mV/s with varying weight ratios (b)**
 39 **Cyclic voltammetry at 20 mV/s (c) Specific capacitance comparison at 20 mV/s and 500 mV/s. System is three electrode**
 40 **with a Pt mesh counter (1.75 cm²), Ag/AgCl reference electrode and 1 M NaNO₃ / H₂O electrolyte.**

41

42 The CVs observed in Figure S2a display a highly rectangular nature indicative of electric double layer
 43 capacitance at a scan rate 500 mV/s with the 90-10 achieving the largest current density [5]. In Figure S2b, multiple scan rate
 44 ranges retain their rectangular nature due to fast charging / discharging over the potential range of 1.1 V [6]. The largest
 45 observed current was clearly for the 90% SWNT- 10% mw rGO composite electrodes with the specific capacitance
 46 calculated at 20 mV/s and 500 mV/s compared in Figure S2c. The 100-0, 95-5, 90-10, 85-15, and 80- 20 ratios (w/w)
 47 obtained the highest specific capacitance ranging between 250 F/g and 306 F/g (mass of active material). Ratios with a
 48 greater weight percent of mw rGO decreased in specific capacitance. The capacitance for the composites at high scan rates of
 49 500 mV/s (Figure S2c) was again relatively high for ratios 100-0, 95-5%, and 90%- 10 ranging between 80 F/g and 120 F/g

50 respectively. Ratios 85-15, 80-20, 50- 50, 40-60, and 0-100 were all significantly lower in specific capacitance at 500 mV/s at
 51 approxiamtely 40 F/g.

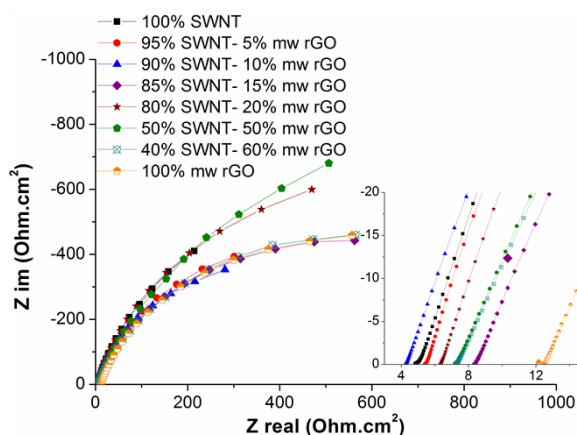
52 The electroactive surface area is calculated. The 90% SWNT-10% mw rGO films had the largest surface area of
 53 52.9 cm². A comparison of the electroactive surface area for all the composites is shown in Table S2 below.

54 **Table S2: Electroactive surface area comparison of the SWNT: mw rGO composite electrodes.**

Composition (w/w%)	Electroactive Surface Area (cm ²)
100% SWNT	43.2
95-5	44.1
90-10	52.9
85-15	34.6
80-20	30.3
50-50	25.9
40-60	25.9
100% mw rGO	25.9

55

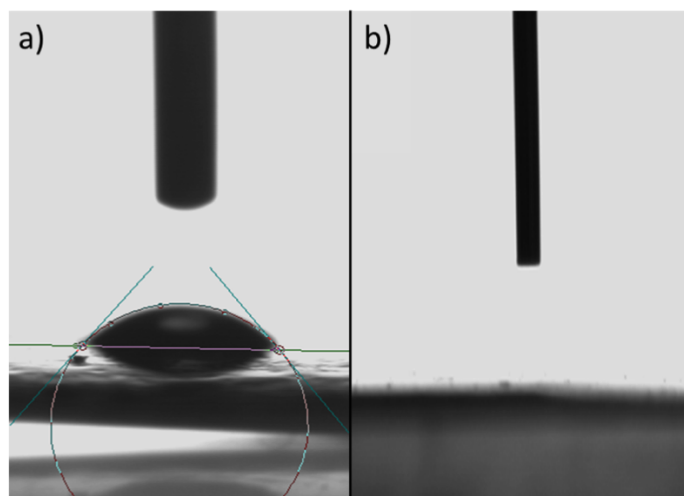
56 In Figure S3, the Nyquist plot comparison is of the SWNT: mw rGO composite electrodes and electrodes of pure
 57 SWNT and pure mw rGO. It can be seen that in the high to middle frequency regime, the imaginary part of the impedance
 58 rapidly rises (near vertical behaviour) with the usually observed semi-circle nearly indistinguishable from the graph
 59 indicating double layer capacitance and fast ion migration during charging / discharging of the electric double layer [5, 7]. In
 60 the inset of Figure S4, the pure mw rGO electrode has the largest series resistance (R_s) of 12.1 Ohm.cm², with R_s
 61 significantly reduced when composites are made. R_s is smallest for the 90-10 film at 4 Ohm.cm².



62

63 **Figure S3: Nyquist plot comparison. System is three electrode with a Pt mesh counter (1.75 cm²), Ag/AgCl reference**
 64 **electrode and 1 M NaNO₃ / H₂O electrolyte. All electrodes have been plasma treated for 20 minutes prior to**
 65 **electrochemical testing. SWNT : mw rGO composite electrodes with varying weight ratios on a Pt sputter coated (100 nm)**
 66 **PVDF membrane.**

67 Contact angle measurements of the 90% SWNT-10%mw rGO composite electrodes (Figure S4a and Figure S4b) prior to
68 (54.5°), and after plasma treatment (<1°) indicate an enhancement in the wettability of the electrodes towards water [8].



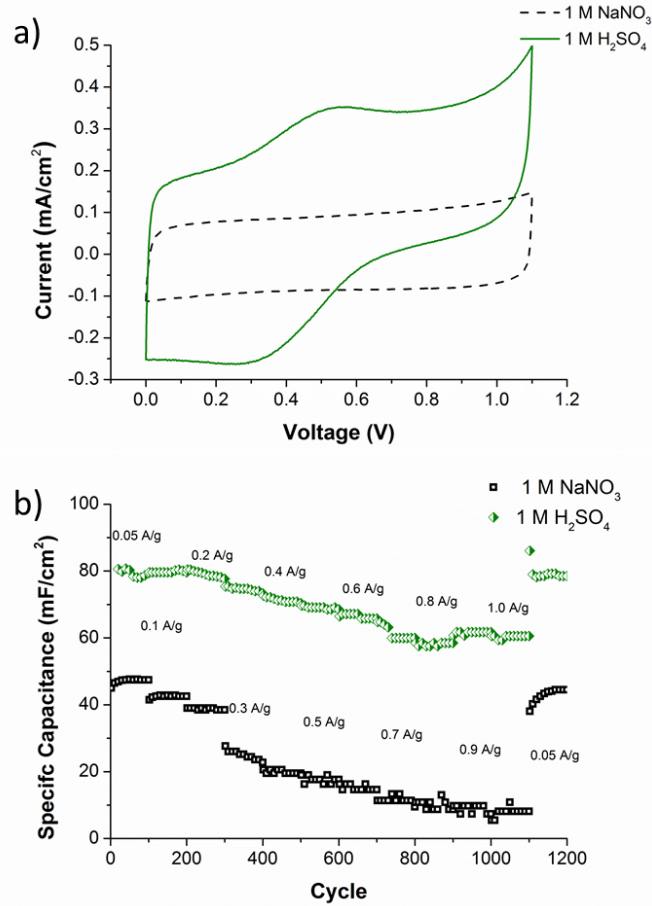
69

70 **Figure S4: Contact angle measurements of 90% SWNT-10% mw rGO film. (a) Before plasma treatment. (b)**
71 **After plasma treatment.**

72 In Figure S5a, the comparison of the CV curves clearly shows that the largest current (green line) is obtained for
73 device electrodes that have been cycled in 1 M H₂SO₄. A large redox peak is observable between 0.3 V and 0.55 V due to
74 redox behaviour associated with the interaction of functional groups of the composite material and the sulphuric acid [9, 10].
75 In Figure S5b, each device was compared using galvanostatic charge / discharge testing (GCD) in order to evaluate long
76 term cycling. It can clearly be seen that for all devices as the current is varied from 0.05 A/g to 1.0 A/g there is a decrease in
77 specific capacitance. The device cycled in 1 M H₂SO₄ has the largest specific capacitance of 80 mF/cm² at 0.05 A/g with a
78 stable response of 61 mF/cm² at 1.0 A/g. When the current was switched back to 0.05 A/g (cycle 1100-1200) the capacity
79 retention was 98%. The device performed significantly less with 1 M NaNO₃ where a rapid decrease in the performance is
80 observed. The sulphuric acid enhances the redox behaviour as it is thought that H⁺ or OH⁻ must be involved in the
81 electrochemical reactions according to the strong dependence of pseudocapacitance on the H⁺ concentration [10].

82

83



84

85 **Figure S5: 90% SWNT-10% mw rGO supercapacitor with each electrode at a thickness of 17 micron. Devices have been**
 86 **optimised by annealing utilising different electrolytes.(a) CV, GCD comparison up to 1.0 A/g.**

87

88 **Equations for Calculations:**

89 Three electrode specific capacitance was calculated from CV using Equation 1 [11], where v is the scan rate in V/s, m is the
 90 mass of the active material of the working electrode, V is the potential difference, and I is the current in A:

$$C_{sp} = \frac{2}{mvV} \int_{-0.2}^{0.9} I dt \quad (1)$$

91

92 Device calculations for specific capacitance, energy density and power density were calculated using the following equations
 93 below:

$$C_{sp} = \frac{2I_d \Delta t_d}{Vk} \quad (2)$$

$$E = \frac{1 C_{sp} V^2}{8 k} \quad (3)$$

$$P = \frac{I_d V}{k} \quad (4)$$

$$P_{max} = \frac{1 V^2}{4(ESR) k} \quad (5)$$

94 Where C_{sp} is the specific capacitance (F), Δt_d is the discharge time (s), V is the potential window (V), I_d is the discharge
 95 current, and the ESR was determined from the intercept of the Nyquist plot (0.21 Ohm.cm²). k can be either the mass of
 96 active material on one electrode; or the electrode volume excluding current collector and separator) that is taken up by the
 97 stacked electrode configuration (cm³).

98 Calculations for electroactive surface area A are as follows;

$$A = \frac{C d}{\epsilon_0 \epsilon_r}$$

99

100

101 Where C is the capacitance (F), d is the typical distance of the electric double layer $\approx 10 \text{ \AA}$ [12], ϵ_0 is the permittivity of free
 102 space $8.854 \times 10^{-12} \text{ Fm}^{-1}$, ϵ_r is the dielectric constant of water 80.1 [12].

103

104 References

- 105 1. Dresselhaus, M.S., et al., *Raman spectroscopy of carbon nanotubes*. Physics Reports, 2005. **409**(2): p. 47-99.
 106 2. Salzmann, C.G., et al., *The Role of Carboxylated Carbonaceous Fragments in the Functionalization and Spectroscopy of a Single-*
 107 *Walled Carbon-Nanotube Material*. Advanced Materials, 2007. **19**(6): p. 883-887.
 108 3. Lota, G., et al., *Carbon materials modified by plasma treatment as electrodes for supercapacitors*. Journal of Power Sources. **195**(22):
 109 p. 7535-7539.
 110 4. S H Shiau, et al., *Growth of a single-wall carbon nanotube film and its patterning as an n-type field effect transistor device using an*
 111 *integrated circuit compatible process*. Nanotechnology, 2008. **19**(10): p. 105303.
 112 5. Bose, S., et al., *Carbon-based nanostructured materials and their composites as supercapacitor electrodes*. Journal of Materials
 113 Chemistry, 2012. **22**(3): p. 767-784.
 114 6. Sun, Y., Q. Wu, and G. Shi, *Graphene based new energy materials*. Energy & Environmental Science, 2011. **4**(4): p. 1113-1132.
 115 7. Rakhi, R.B., et al., *High performance supercapacitors using metal oxide anchored graphene nanosheet electrodes*. Journal of Materials
 116 Chemistry, 2011. **21**(40): p. 16197-16204.
 117 8. Chau, T.T., et al., *A review of factors that affect contact angle and implications for flotation practice*. Advances in Colloid and Interface
 118 Science, 2009. **150**(2): p. 106-115.
 119 9. Huang, Z.-D., et al., *Effects of reduction process and carbon nanotube content on the supercapacitive performance of flexible graphene*
 120 *oxide papers*. Carbon, 2012. **50**(11): p. 4239-4251.
 121 10. Chen, Q.-L., et al., *Fabrication and electrochemical properties of carbon nanotube array electrode for supercapacitors*. Electrochimica
 122 Acta, 2004. **49**(24): p. 4157-4161.
 123 11. Guo, H. and Q. Gao, *Boron and nitrogen co-doped porous carbon and its enhanced properties as supercapacitor*. Journal of Power
 124 Sources, 2009. **186**(2): p. 551-556.
 125 12. J. Koryta, J.D., L. Kavan, *Principles of Electrochemistry 2nd Edition*. 1993: John Wiley & Sons Inc.

126

127